

Percolation and critical $O(n)$ loop configurations

Chengxiang Ding¹, Youjin Deng^{2†}, Wenan Guo^{1†}, and
Henk W.J. Blöte³

¹Physics Department, Beijing Normal University, Beijing 100875, P. R. China

²Hefei National Laboratory for Physical Sciences at Microscale, Department of
Modern Physics, University of Science and Technology of China, Hefei 230027,
China

³ Instituut Lorentz, Leiden University, P.O. Box 9506, 2300 RA Leiden, The
Netherlands

Abstract. We study a percolation problem based on critical loop configurations of the $O(n)$ loop model on the honeycomb lattice. We define dual clusters as groups of sites on the dual triangular lattice that are not separated by a loop, and investigate the bond-percolation properties of these dual clusters. The universal properties at the percolation threshold are argued to match those of Kasteleyn-Fortuin random clusters in the critical Potts model. This relation is checked numerically by means of cluster simulations of several $O(n)$ models in the range $1 \leq n \leq 2$. The simulation results include the percolation threshold for several values of n , as well as the universal exponents associated with bond dilution and the size distribution of the diluted clusters at the percolation threshold. Our numerical results for the exponents are in agreement with existing Coulomb gas results for the random-cluster model, which confirms the relation between both models. We discuss the renormalization flow of the bond-dilution parameter p as a function of n , and provide an expression that accurately describes a line of unstable fixed points as a function of n , corresponding with the percolation threshold. Furthermore, the renormalization scenario indicates the existence, in p versus n diagram, another line of fixed points at $p = 1$, which is stable with respect to p .

PACS numbers: 05.50.+q, 64.60.Cn, 64.60.Fr, 75.10.Hk

† Corresponding authors: waguo@bnu.edu.cn, yjdeng@ustc.edu.cn

1. Introduction

The reduced Hamiltonian of the $O(n)$ spin model is usually written as

$$\mathcal{H}/(k_B T) = -J/(k_B T) \sum_{\langle ij \rangle} \vec{S}_i \cdot \vec{S}_j, \quad (1)$$

where k_B is the Boltzmann constant, and T the temperature. The spin \vec{S}_i is an n dimensional vector, localized at site i of a lattice. The sum is over all nearest-neighbor pairs. For the special cases $n = 1, 2, 3$, this model corresponds to the Ising, the XY and the Heisenberg model, respectively.

The $O(n)$ symmetry actually allows a more general form of the pair interaction—e.g., one may replace $J/(k_B T) \vec{S}_i \cdot \vec{S}_j$ by $a(\vec{S}_i \cdot \vec{S}_j)$ with a an analytic function. A particularly useful choice [1] is $a \equiv \ln(1 + x \vec{S}_i \cdot \vec{S}_j)$, where x is a temperature-like variable. The so-called high-temperature graph expansion [2] for such a model yields a weighted sum of graphs, in which each site connects to its neighboring sites by an *even* number of ‘bonds’. On lattices with coordination number of at most three, like the honeycomb lattice, these graphs reduce to a set of non-intersecting loops. For properly normalized $O(n)$ spins, the resulting partition sum reads [1]

$$Z_{\text{loop}} = \sum_{\mathcal{G}} x^{N_b} n^{N_l}, \quad (2)$$

where the sum is over all possible loop configurations \mathcal{G} that can be constructed on the edges of the lattice. The number of ‘bonds’, i.e., edges covered by \mathcal{G} , is denoted as N_b , and the number of loops in \mathcal{G} as N_l . Remarkably, the spin dimensionality n of the original model now appears as a continuous variable. The critical point of this model is exactly known for $-2 \leq n \leq 2$, as well as some critical exponents [3].

The significance of clusters in critical or near-critical configurations of $O(n)$ and q -state Potts models has already been recognized long ago [4, 5, 6]. While the present work focuses on the percolation aspects of the two-dimensional $O(n)$ model, we consider it useful to first review the similar case of the two-dimensional Potts model.

It is well known that the critical singularities of the ferromagnetic q -state Potts model can be correctly represented in terms of Kasteleyn-Fortuin (KF) clusters [5, 6], also called random clusters, rather than in terms of naively defined Potts clusters. The latter are formed by connecting, with probability 1, nearest-neighbor spins in the same Potts state, while the formation of KF clusters uses a probability $p = 1 - e^{-K}$ instead, where K is the nearest-neighbor coupling constant of the Potts model. Thus, one may consider KF clusters as percolation clusters formed by a bond-percolation process that uses the Potts clusters as a substrate.

Both the size of the largest Potts and that of the largest KF cluster diverge at the critical point, but it is the size of the KF cluster that determines the spontaneous magnetization, governed by the order-parameter exponent $\beta(q)$. The Potts magnetic correlation function appears to be equal to the probability that the correlated sites belong to the same KF cluster. It follows that the fractal dimension d_f of KF clusters is equal to the Potts magnetic renormalization exponent y_h [7]. Potts clusters are denser than KF clusters, and are described by a larger fractal dimension [8, 9]. At the Potts critical coupling K_c , bond dilution of Potts clusters yields a percolation threshold at bond probability $p = 1 - e^{-K_c}$ [7, 9, 10], which corresponds precisely with KF clusters. In the renormalization language, this KF point acts as an unstable

fixed point on the Potts critical line parametrized by p , and the Potts clusters are described by a stable fixed point at larger p .

For the case of the tricritical q -state Potts model, which can be reached from the pure q -state Potts model by including vacant sites [11, 12], the situation is somewhat different. The thermodynamic singularities are still described by KF clusters, which are obtained by bond dilution of tricritical Potts clusters with bond probability $p = 1 - e^{-K_t}$, where K_t is the Potts coupling at the tricritical point. But the percolation threshold of the bond dilution process no longer coincides with the KF point. The percolation threshold now occurs at $p < 1 - e^{-K_t}$, and marks an unstable fixed point with respect to variation of p . The fractal properties of tricritical Potts clusters, as well as those of KF clusters, are now described by a fixed point that is stable in the p direction.

Furthermore, the pair of fixed points on the tricritical line can be related to the pair on the critical line. When we define q' as the number of states for which the tricritical Potts model has the same conformal anomaly as the q -state critical Potts model, it is found that the universal properties of q -state Potts clusters match those of q' -state tricritical KF clusters, and that q -state KF clusters correspond with diluted tricritical q' -state clusters at the percolation threshold [9, 13].

It is now natural to address a similar percolation problem defined within the domains separated by critical $O(n)$ loops. In particular, one may ask the questions for what bond probability p there will be a percolation threshold, what is the exponent associated to p , and what is the fractal dimension of the percolation clusters at the threshold. While it is possible to find direct answers for the honeycomb $O(1)$ model, this work will address these questions also for other values of n . In Sec. 2 we predict the exponent y_h , which is the fractal dimension of the clusters at the percolation threshold, and y_p , or, $\nu_p = 1/y_p$, which controls the divergence of the percolation correlation length as $\xi = (p - p_c)^{-1/y_p}$. Section 3 provides a numerical analysis that yields the percolation thresholds and a verification of the Coulomb gas result. The analysis is based on finite-size scaling [14] and Monte Carlo simulations of $O(n)$ models for several values of n , using a recently developed cluster algorithm [15]. In Sec. 4 we review the self-matching lattice argument for the case of the dual triangular lattice, and its consequences for our percolation problem. We conclude with a short discussion in Sec. 5.

2. Bond percolation between dual spins

In defining the percolation problem of $O(n)$ loop configurations, it is convenient to make use of the representation of such configurations by means of Ising spins on the dual lattice. Spins not separated by a loop are given the same sign, and spins separated by one loop have opposite signs. Here we ignore the possible inconsistency of such an assignment with the existence of periodic boundary conditions, because we expect that leading critical singularities are not modified by the restriction that the spins are single valued. The dual Ising configuration thus completely specifies the loop configuration (but we do not attempt to express the $O(n)$ partition sum in the Ising language). We can now construct dual clusters by drawing, with probability 1, bonds between nearest-neighbor sites occupied by spins in the same state. The hulls of these clusters are the $O(n)$ loops. At criticality of the $O(n)$ loop model, the clusters are fractals with dimension d_a , and the hulls are fractals with dimension d_t .

On the basis of a critical loop configuration, one may now connect neighboring

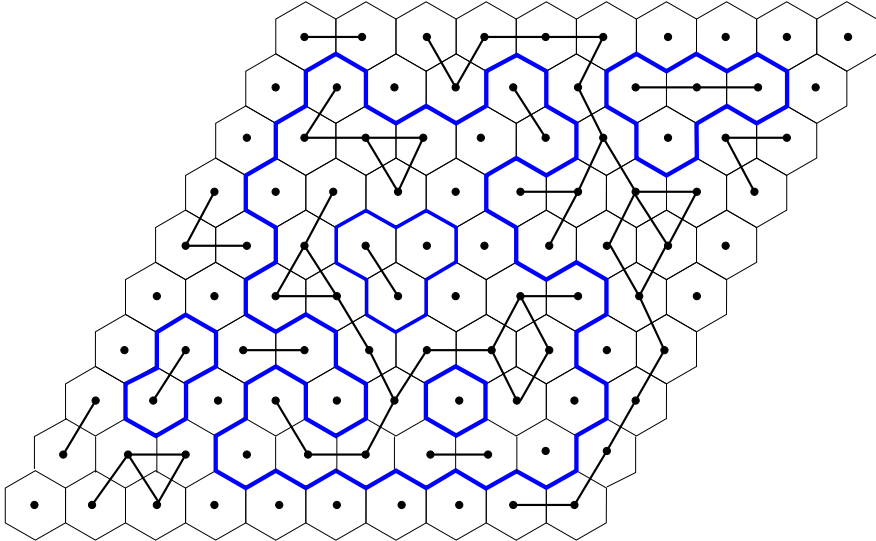


Figure 1. An $O(n)$ loop configuration on the honeycomb lattice, together with a bond percolation configuration in dual clusters as defined within $O(n)$ loops.

dual Ising spins in the same state instead with a bond probability $p < 1$ and thus form new types of clusters. This is illustrated in Fig. 1.

The results for the percolation problem on Potts clusters described in Sec. 1 are relevant for the analysis of the geometric aspects of critical $O(n)$ loop configurations, because of the well-known relation between critical $O(n)$ loops and the hulls of tricritical random-cluster configurations [3, 16]. As a result, the magnetic exponent of the tricritical Potts model is equal to the fractal dimension of the regions separated by loops in the corresponding $O(n)$ model on the surrounding lattice. Although it is not obvious how to interpret the $O(n)$ loops on the honeycomb lattice as the hulls of a KF random-cluster model, one may assume that the universal aspects of the percolation problems within the regions separated by the loops are independent of the details of the lattice structure. Moreover, the partition sum of the critical $O(n)$ loop model on the honeycomb lattice was shown to be identical to that of a tricritical Potts model with vacancies [12] on the triangular lattice. This mapping identifies the $O(n)$ loops with the hulls of tricritical Potts clusters. As mentioned above, the universal properties of the tricritical Potts clusters also apply to tricritical KF clusters. One can thus associate the fractal dimension d_l of critical $O(n)$ loops with the hull fractal dimension of tricritical KF clusters, and the fractal dimension d_a of the regions separated by loops with the fractal dimension of tricritical KF clusters.

These exponents are exactly known by means of the Coulomb gas method [17, 18, 19], and verified numerically [20] for the $O(n)$ model. The critical $O(n)$ loop model and the equivalent $q = n^2$ -state tricritical Potts model share the Coulomb gas coupling g , which is given by the following equation

$$q = 4 \cos^2(g\pi), \quad 1 \leq g \leq 2. \quad (3)$$

Let $g' \equiv 1/g$, thus $0.5 \leq g' \leq 1$, be the Coulomb gas coupling of the q' -state critical Potts model, where q' is determined by

$$q' = 4 \cos^2(g'\pi). \quad (4)$$

This q' -state critical Potts model has the same conformal anomaly as the critical $O(n)$ loop model, as well as the n^2 -state tricritical Potts model [21, 22]:

$$c = 1 - \frac{6(1-g)^2}{g} = 1 - \frac{6(1-g')^2}{g'} . \quad (5)$$

As already mentioned in Sec. 1, the Potts clusters of this q' -state critical Potts model are equivalent with the q -state KF clusters of the tricritical Potts model, and therefore also with the regions separated by critical $O(n)$ loops. Just as the process of bond dilution of critical q' -state Potts clusters leads to KF random clusters, we expect that bond dilution of the dual clusters defined within $O(n)$ loops will, at the bond percolation threshold, lead to configurations with critical KF-like universal properties. The fractal dimension of the KF clusters of the critical q' -state Potts model is [19]

$$y_h = 1 + g'/2 + 3/(8g') , \quad (6)$$

which can be continued analytically into the tricritical range [23]. This holds as well for the bond-dilution exponent, which is given by [24]

$$y_p = 1 - 3g'/2 + 1/(2g') . \quad (7)$$

For the special values $n = 0, 1$ and 2 it is possible to derive exact percolation thresholds. For $n = 0$, loops are in fact forbidden due to their zero weights, but, depending on the boundary conditions, loop segments may emerge from the boundaries. In the high-temperature $O(0)$ phase, these segments will, however, be confined to a boundary layer of finite thickness, and the bulk of the model will be empty. Therefore, the percolation threshold is exactly that of the triangular bond-percolation model, which is given as the solution of

$$p^3 - 3p + 1 = 0 . \quad (8)$$

Assuming continuity of the percolation threshold between the high-temperature $O(n)$ phase and the critical state, the bond-percolation threshold $p_c(n = 0)$ at $O(0)$ criticality is also equal to the solution of Eq. (8), which is

$$p_c(n = 0) = 2 \sin(\pi/18) \quad (9)$$

For the $O(1)$ loop model, one may apply an exact duality transformation which yields the critical triangular Ising model. Thus, the dual Ising configurations described above are precisely those of the critical triangular Ising model and we can use its known properties. The critical point of the triangular model [25] is $K_c = (1/4) \ln 3$, and its random-cluster representation determines the percolation threshold as

$$p_c(n = 1) = 1 - \exp(-2K_c) = 1 - 1/\sqrt{3} . \quad (10)$$

For the case $n = 2$ we apply an argument of a different nature. First we note that, along the Potts critical line as parametrized by p , the two fixed points, describing the Potts and KF clusters respectively, merge [9] for $q \rightarrow 4$, the point where the Potts critical and tricritical branches meet. At this point, the difference between the critical and tricritical KF clusters vanishes. Therefore we expect that no further bond dilution of the aforementioned dual clusters is required, i.e.,

$$p_c(n = 2) = 1 . \quad (11)$$

The predictions for the percolation thresholds at $n = 1$ and 2 will be the subject of numerical verification in Sec. 4.3.

3. Simulation

3.1. Sampled variables and finite-size scaling

The representation of the Potts model by means of KF clusters has led to the development of cluster Monte Carlo algorithms [26, 27], which drastically reduce the critical slowing down problem in simulations of the Potts model. Since then, more cluster algorithms have been developed, so that accurate simulation results can now be obtained for a considerable number of other critical model systems. Here we use an efficient cluster algorithm [15] for $O(n)$ loop models with noninteger $n > 1$ to verify the predictions made in Sec. 2. The simulations took place at the critical point which is given by $x_c = [2 + (2 - n)^{1/2}]^{-1/2}$ for the honeycomb lattice [3]. The loop model cluster algorithm [15] easily allows meaningful simulations up to a linear system size $L = 512$ at the critical point.

The configurations generated by the Monte Carlo algorithm are represented by means of dual Ising spins. The percolation problem involves the addition of bonds between equal nearest-neighbor Ising spins with probability p . For this percolation problem on the dual clusters, we expect, at least in part, a similar behavior as a function of p as usual in percolation theory [28]. Thus, for small p the percolation clusters are small, and they will grow with increasing p until the percolation threshold p_c where the largest percolation cluster diverges, at least in the thermodynamic limit. In a finite system, the largest cluster is limited by the system size. When a percolation cluster reaches the system size, we call it a “spanning cluster”. However, this statement has to be made more precise. For a finite system with periodic boundary conditions, there are different rules to define a spanning cluster. One may define it as a cluster whose linear size in at least one of the lattice directions reaches the size of the periodic box, or as a cluster that connects to itself along *at least* one of the periodic directions [29]. Here we use the latter definition.

In order to obtain the threshold p_c and some critical exponents associated with this percolation problem, several quantities are sampled. These include the susceptibility-like quantity χ_G , the probability R_e that the occupied bonds form a nontrivial loop ('nontrivial' means here that the loop spans the torus and thus cannot be shrunk into a point by a continuous deformation), and the density P_∞ of the spanning cluster. The quantity R_e is alternatively called the wrapping or the crossing probability. We provide some further details to describe these quantities.

On the triangular lattice, a cluster may span the system in different directions, including the ones labeled x , y and z in Fig. 2. We thus define the measure R_e of the spanning probability as

$$R_e = \langle (R_x + R_y + R_z)/3 \rangle, \quad (12)$$

where $\langle \dots \rangle$ stands for ensemble averaging, and the subscript e means that a connection can exist along each of the x , y , and the z directions. If there is no cluster that spans the system, we put $R_x = R_y = R_z = 0$. We put $R_x = 1$ if there exists of a cluster that connects to itself over a displacement equal to a unit vector along the x direction; if there are no other connections to itself in other directions, we put $R_y = R_z = 0$. The same applies with cyclic permutations of x , y , and z . However, a cluster may also connect to a periodic image of itself in other directions than those of the x , y , and z axes. If the cluster connects to itself with a nonzero displacement vector that is not parallel to the x , y , or z direction, we put $R_x = R_y = R_z = 1$. With this definition of

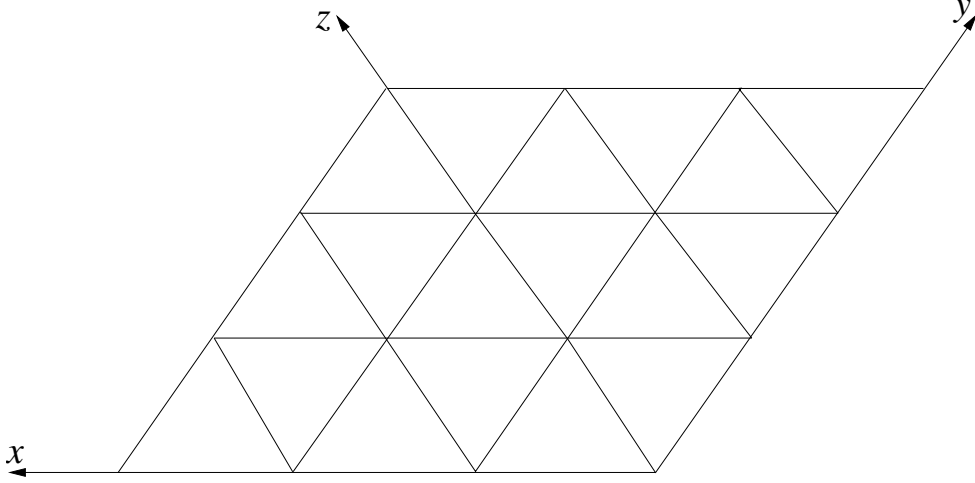


Figure 2. A percolation cluster may span the periodic system with hexagonal symmetry in the x , y and z direction.

R_e , the x , y , and z directions are treated equivalently, despite the fact that there are only two independent directions in two dimensions.

Finite-size scaling yields the following finite-size behavior for R_e as a function of the finite size L and the bond probability:

$$R_e = R_{ec} + a(p - p_c)L^{y_p} + \dots + b_1L^{y_1} + b_2L^{y_2} + \dots, \quad (13)$$

where p_c is the percolation threshold, y_p is the bond-dilution exponent, and y_1, y_2, \dots are negative correction-to-scaling exponents. The quantity R_{ec} is defined as the value of R_e at p_c , which is also universal [30, 31], but still dependent on the finite system geometry and, at present, on the underlying $O(n)$ critical state.

The percolation susceptibility χ_G and the percolating cluster density P_∞ are defined as

$$\chi_G = L^{-d} \left\langle \sum_i^{N_c} n_i^2 \right\rangle, \quad (14)$$

$$P_\infty = L^{-d} \left\langle n_\infty \right\rangle \quad (15)$$

respectively, where $d = 2$ represents the dimensionality of the model, and N_c is the number of clusters. The number of sites in the i -th cluster is denoted n_i , and n_∞ refers to that in the spanning cluster. Thus P_∞ represents the probability that a randomly chosen site belongs to the spanning cluster. The definition of χ_G is the same as the Potts magnetic susceptibility, expressed in terms of an ensemble average over random clusters.

Finite-size scaling predicts the following behavior for P_∞ and χ_G :

$$P_\infty = L^{y_h - d} (a_0 + a_1(p - p_c)L^{y_p} + \dots + b_1L^{y_1} + b_2L^{y_2} + \dots), \quad (16)$$

$$\chi_G = L^{2y_h - d} (a_0 + a_1(p - p_c)L^{y_p} + \dots + b_1L^{y_1} + b_2L^{y_2} + \dots), \quad (17)$$

where y_h is the fractal dimension of the percolating cluster. At the percolation threshold p_c , these equations reduce to

$$P_\infty = L^{y_h - d} (a_0 + b_1L^{y_1} + b_2L^{y_2} + \dots), \quad (18)$$

and

$$\chi_G = L^{2y_h-d}(a_0 + b_1 L^{y_1} + b_2 L^{y_2} + \dots). \quad (19)$$

3.2. Results

We illustrate the numerical procedure, using the $O(1.5)$ loop model as an example. The model with periodic boundary conditions was simulated at its critical point [3], which is $x_c = 0.60778 \dots$. Since the cluster algorithm hardly suffers from any critical slowing down, as described in Ref. [15], samples were taken at intervals of only 2 cluster steps.

The first stage involved the determination of the spanning probability $R_e(p, L)$, the density P_∞ of the percolating cluster, and the percolation susceptibility χ_G for several values of the bond probability p . This was done for 6 system sizes L ranging from 8 to 256. After the equilibration of the system, 10^8 samples were taken for each value of p in the range $8 \leq L \leq 64$, and 4×10^7 samples in the range $64 < L \leq 256$. Statistical errors were estimated by dividing each run in 1000 partial results, and subsequent statistical analysis. The correlations between subsequent partial results are negligible for the lengths of these runs. Parts of the R_e data are shown in Fig. 3.

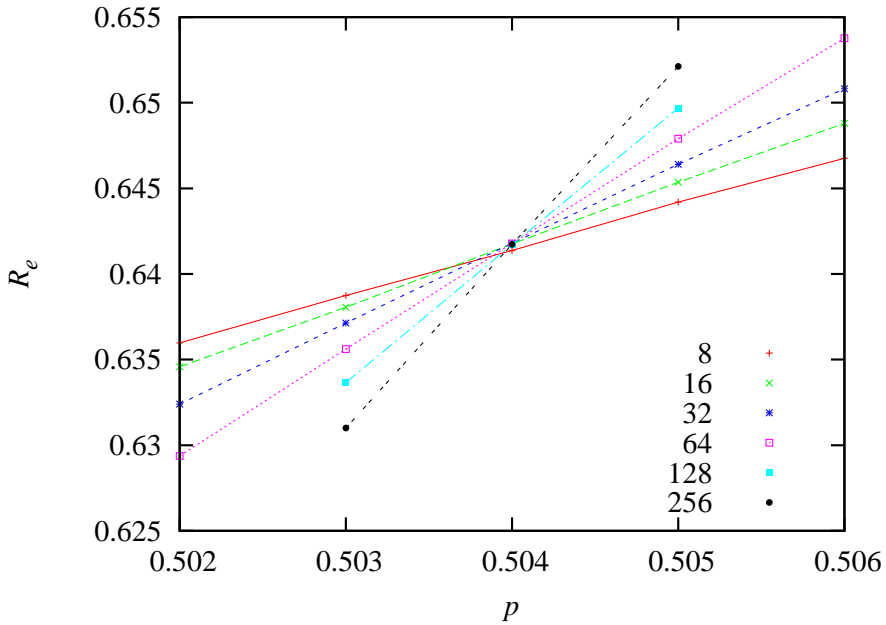


Figure 3. Spanning probability R_e versus bond probability p for various system sizes in the case $n = 1.5$. The lines connecting the data points are added only for illustration. All error bars are much smaller than the size of the data points.

The number of free parameters in the finite-size scaling equations (13), (16) and (17) makes it necessary to apply a multivariate method. We used the Levenberg-Marquardt least-squares algorithm, which allows nonlinear fits according to these equations. We thus determined the percolation threshold p_c from the R_e versus p data. The next step involved a simulation of seven system sizes in the range

$8 \leq L \leq 512$ at our estimated value of p_c , with the same lengths as mentioned above for $8 \leq L \leq 256$, and 10^7 samples for $L = 512$. Including these runs, we fitted the unknowns in the finite-size scaling formula Eq. (13), also including the universal probability R_{ec} and the dilution exponent y_p to the data. This yielded our final estimates, namely $p_c = 0.50403$ (1), $R_{ec} = 0.6420(2)$, and $y_p = 0.395$ (2) for the bond-dilution exponent. The latter result is in a good agreement with the Coulomb gas prediction $y_p = 0.3955 \dots$.

Since the analysis of the data for the density P_∞ of the percolating cluster and for the percolation susceptibility χ_G yielded the p dependence in terms of the coefficients a_i , we can deduce the value of P_∞ and χ_G at our best estimate for the percolation threshold. Parts of these data for P_∞ are shown in Fig. 4 versus L . We

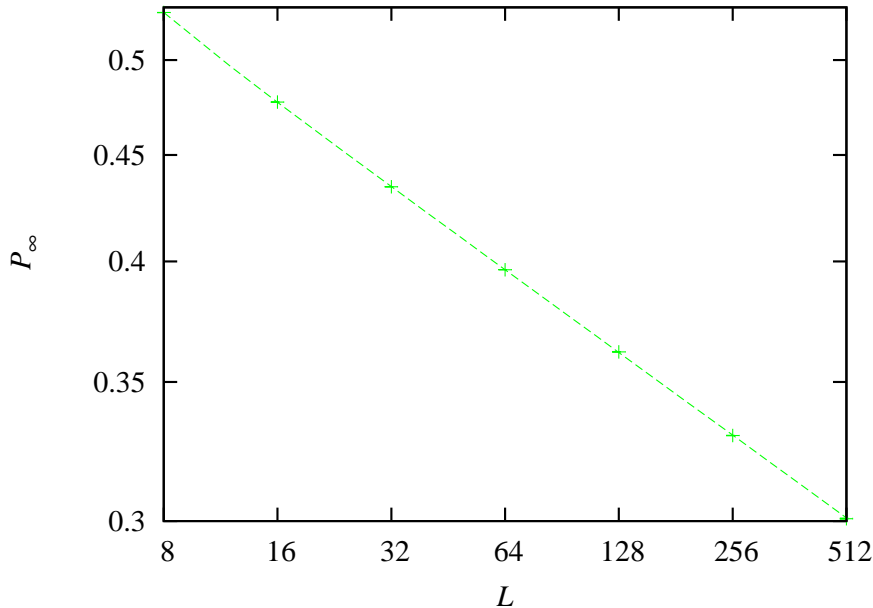


Figure 4. Density P_∞ of the spanning cluster at the percolation threshold versus system size L for the case $n = 1.5$, shown on logarithmic scales. The dashed line represents a fit to the data points according to Eq. (18). The error bars are much smaller than the size of the data points.

find that, at the percolation threshold, P_∞ and χ_G are well described by power laws as a function of sufficiently large lattice sizes L , in agreement with the finite-size scaling behavior expressed by Eqs. (18) and (19). A fit of the numerical data for P_∞ and χ_G according to these equations yields the fractal dimension y_h of the percolation clusters as $y_h = 1.8678$ (2) and $y_h = 1.8678$ (1) respectively. Both values are in a good agreement with the value $1.86775 \dots$ based on the Coulomb gas prediction, Eq. (6).

The same procedure as described above was applied to the cases $n = 1.0, 1.25, \sqrt{2}, 1.5, 1.75, 1.90$ and 1.95 . The percolation thresholds p_c , the bond-dilution percolation exponent y_p , and the fractal dimensions of the percolation cluster y_h are obtained similarly. The results are listed in Table 1. The exponents are in a satisfactory agreement with the values predicted by Eqs. (6) and (7).

We also performed simulations for $n = 2$. However, the R_e versus p data, which

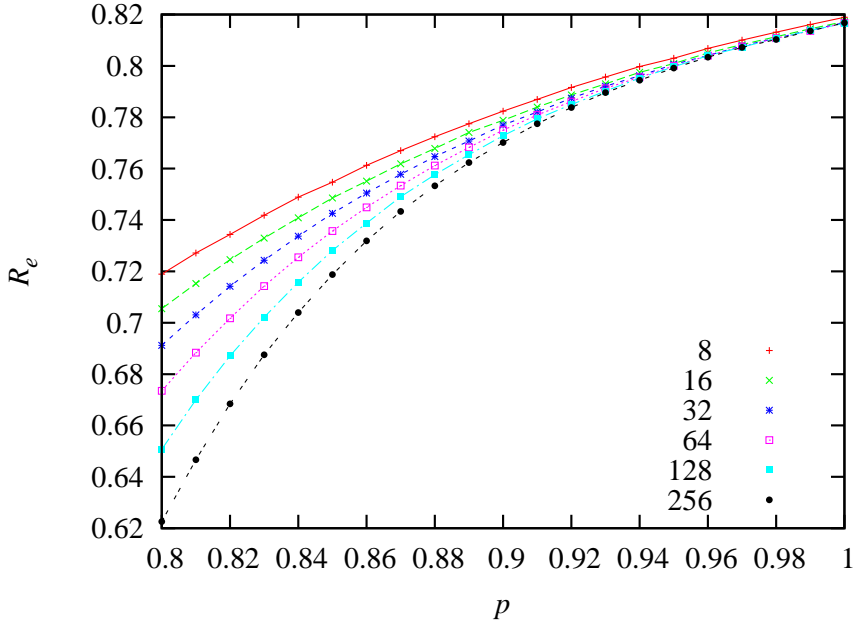


Figure 5. Spanning probability R_e versus bond probability p for various system sizes in the case $n = 2$. The lines connecting the data points are added only for illustration.

are shown in Fig. 5, do not show intersections for different system sizes. Near $p = 1$, the curves appear to run asymptotically parallel at vanishing distances for large L . These findings are consistent with the predicted values $p_c = 1$ and $y_p = 0$. However, the vanishing of y_p renders Eq. (13) insufficient for a numerical determination of p_c from the R_e data for $n = 2$. We thus fitted the exponent y_h using the data for P_∞ and χ_G at the theoretical value $p_c = 1$. These results are included in Table 1. Before attempting a numerical analysis of the R_e data, we will adapt Eq. (13) for the case of a marginally relevant bond dilution field, with the help of renormalization considerations in Sec. 4.

4. Self-matching argument and renormalization flow

4.1. Matching property

First we shall briefly review the matching properties [32, 33] of planar lattices and the consequences for the site-percolation thresholds of some of these lattices. Let $\mathcal{P} \equiv (\mathcal{V}, \mathcal{A})$ be a planar lattice, where \mathcal{V} is the set of lattice sites and \mathcal{A} the set of edges connecting the nearest-neighbor sites of \mathcal{V} . The faces of this lattice are polygons without any ‘diagonals’. Let \mathcal{B} be the set of diagonals connecting all pairs of non-nearest-neighboring sites within each polygon. Then, we define the lattice \mathcal{L} , in which these diagonals are included, as $\mathcal{L} \equiv (\mathcal{V}, \mathcal{A} + \mathcal{B})$. Then, \mathcal{P} and \mathcal{L} are called matching lattices. It is possible to define matching lattices in a more general way, but that is unnecessary for our present purposes.

Suppose that a given site-percolation configuration on \mathcal{P} percolates in the \vec{x}

lattice direction. The existence of a percolating path prevents the existence of a percolating path in a conjugate percolation configuration obtained as follows. Replace the occupied sites of \mathcal{V} by empty sites, and vice versa. Add the diagonals, leading to the lattice \mathcal{L} , and consider the percolation problem in the other lattice direction denoted \vec{y} . It then follows that there is no percolating path in that direction. Furthermore, if a given configuration of site variables on \mathcal{P} does not lead to a percolating path in the \vec{x} direction, then the conjugate problem must have a percolating path in the \vec{y} direction. As a consequence, if the site percolation threshold of lattice \mathcal{P} is $p_{\mathcal{P}}^{(s)}$, and the site percolation threshold of the lattice \mathcal{L} is $p_{\mathcal{L}}^{(s)}$, then the thresholds are related as

$$p_{\mathcal{P}}^{(s)} + p_{\mathcal{L}}^{(s)} = 1. \quad (20)$$

Since no ‘diagonals’ can be added into the triangular lattice, the triangular lattice is called a self-matching lattice, and the difference between the two thresholds in Eq. (20) vanishes. The matching argument thus yields that the percolation threshold of the triangular lattice, as well as that of other self-matching lattices, lies at $p_c^{(s)} = 1/2$.

An important feature of the matching argument is its independence of interactions between the site variables, as long as these interactions are symmetric under the interchange of occupied and unoccupied lattice sites.

4.2. Percolation at bond probability $p = 1$

For the case $n = 1$ and bond probability $p = 1$, the model reduces to the Ising model on the triangular lattice with coupling $K = -(\ln x)/2$, and all neighboring sites with equal spins are connected by occupied bonds. The $x < x_c = 1/\sqrt{3}$ region corresponds to the low-temperature ferromagnet, and $1 \geq x \geq x_c$ to the high-temperature ferromagnet, and $x > 1$ to the antiferromagnet. Thus, the symmetry between $+$ and $-$ spins holds in the range $x \geq x_c$. If one considers $+$ spins as occupied sites, and $-$ spins as unoccupied ones, the bond percolation model with $p = 1$ can be regarded as a correlated site percolation model with site-occupation probability $p^{(s)} = 1/2$. In particular, the $x = 1$, i.e., $K = 0$ case reduces to the standard site percolation on the triangular lattice [17]. The aforementioned self-matching relation tells us that the whole line for $p = 1$ and $x \geq x_c$ is a critical line of the percolation type, as already noted in Ref. [34]. Figure 5 in the latter reference describes the renormalization flow of the model in the p versus K plane. Since the percolation critical line must be a flow line, it follows that, at the Ising critical temperature, the point $p = 1$ is a fixed point. Since the KF fixed point is unstable, and there is no sign of intermediate fixed points [34], the $p = 1$ fixed point is stable along the p direction.

For $n \neq 1$, the $O(n)$ loop model involves non-local interactions, as reflected by the quantity N_l in Eq. (2). Nevertheless, the symmetry between the $+$ and $-$ spins in the dual triangular lattice still holds as long as $x \geq x_c(n)$. The matching argument yields that, for $n \leq 2$, the point $p = 1, x = x_c(n)$ is always a fixed point for the flow along the p direction.

Consider the subspace (n, p) with $x = x_c(n)$ in the three-parameter space (n, p, x) . We have now derived two lines of fixed points as a function of n , namely $p = 1$ from the self-matching argument, and $p = p_c(n)$ from our numerical estimates. The latter seems to be tangent to the line $n = 2$, while the former is perpendicular to the $n = 2$ line. This tells something about the renormalization flow near $n = 2$.

According to the aforementioned results, we conjecture the associated renormalization flow as shown in Fig. 6. For $n = 2$, the bond-dilution field is marginally relevant for $p < 1$ and marginally irrelevant $p > 1$. The lowest order

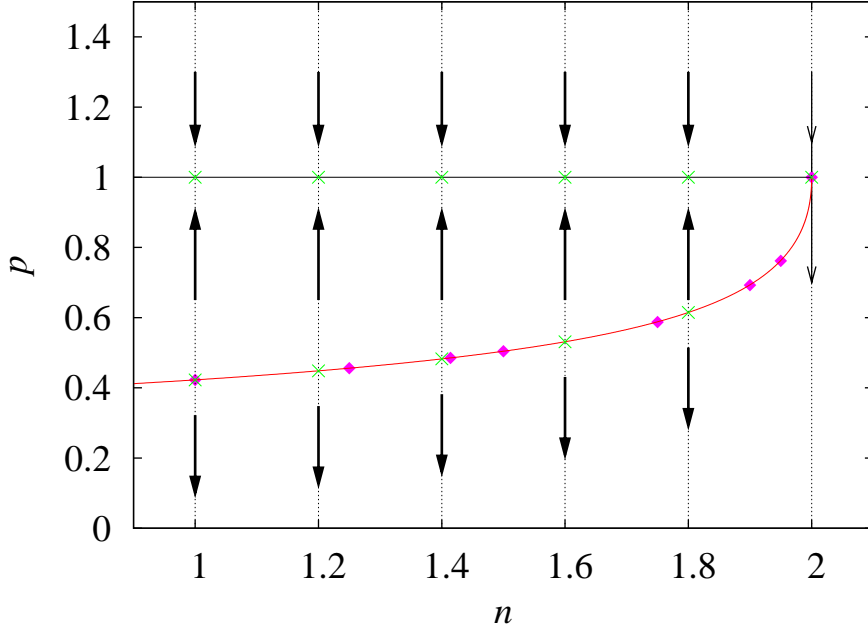


Figure 6. Percolation threshold $p_c(n)$ and the conjectured renormalization flow. The numerical estimates of $p_c(n)$ are shown as diamonds, and the \times symbols stand for the fixed points. The renormalization flow is represented by the arrows, and for $n = 2$ we use the thin arrows for the marginally relevant field. The curve is given by Eq. (25) with $a_0 = 0.486, a_1 = 1.5$.

renormalization equation in $\Delta p \equiv 1 - p$ and $\sqrt{\Delta n} \equiv \sqrt{2 - n}$ leading to the flow diagram sketched in Fig. 6 is

$$\frac{d\Delta p}{dl} = r_0 \Delta p \sqrt{\Delta n} + r_1(\Delta p)^2 \quad (21)$$

where l parametrizes the renormalization flow such that the rescaling factor is e^l , and r_0 and r_1 are unknown constants. The appearance of $\sqrt{\Delta n}$ in this equation is in line with the dependence of the $O(n)$ critical point x_c and that of the Coulomb gas coupling constant g on n .

4.3. Numerical evidence for the conjectured fixed points at $p(n) = 1$

If the line of stable fixed points is indeed located at $p(n) = 1, x = x_c(n)$ for $0 \leq n \leq 2$, the amplitude of the irrelevant bond-dilution field is zero at and only at $p = 1$. For a test, we simulated the critical $n = 1.5$ loop model near $p = 1$. The bond-dilution exponent is given by Eq. (7), where the Coulomb-gas couplings for the stable and unstable fixed points relate as $gg' = 1$. For $n = 1.5$ this yields the bond-dilution exponent as $y'_p = -0.4386$ near $p = 1$ and $y_p = 0.3955$ near the threshold p_c .

Parts of the R_e data near $p = 1$ are shown in Fig. 7 versus the bond-occupation probability p . The R_e data lines become more and more flat when size L increases,

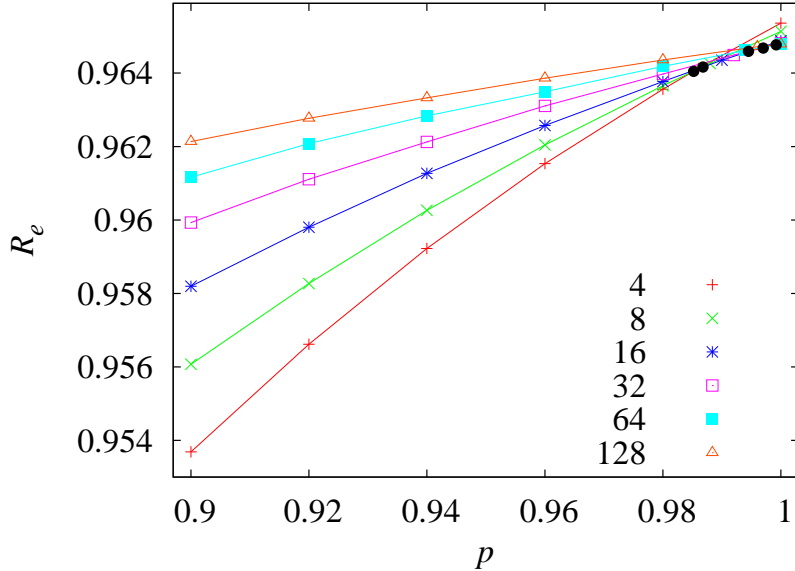


Figure 7. Spanning probability R_e for $n = 1.5$ and near $p = 1$ vs. the bond-occupation probability p . The labels represent linear size L . The filled circles approximately locate at intersections of the L and the $2L$ data lines with $L = 4, 8, 16, 32, 64$. They rapidly approach to $p = 1$.

reflecting that the bond-dilution field is irrelevant. The filled circles mark the intersections of the L and the $2L$ data lines with $L = 4, 8, 16, 32$ and 64. They are approaching $p = 1$ when L increases, suggesting that $p = 1$ is indeed a stable fixed point. To obtain more solid evidence, we fitted the R_e data at $p = 1$ by $R_e(L) = R_{e1} + bL^{y_c}$, and obtained $R_{e1} = 0.964780$ (8) and $y_c = -1.9$ (2), which indicates the absence of finite-size corrections with exponent $y'_p = -0.4386$.

The data are also shown in Fig. 8 as $|R_e(L, p) - R_{e1}|$ versus L , where $R_{e1} = 0.964780$ was taken from the fit. This figure illustrates that the difference $|R_e(L, p) - R_{e1}|$ at $p = 1$ vanishes much more rapidly than that for $p \neq 1$. It also rather clearly demonstrates that the finite-size correction exponent is independent of the bond-occupation probability p when $p \neq 1$, and that its value is in agreement with the expected value $y'_p = -0.4386$.

We observed that the R_e data in range $10 \leq L \leq 512$ can be well described by

$$R_e(p, L) = R_{e1} + a_1(p - p_{c1})L^{y'_p} + a_2(p - p_{c1})^2L^{2y'_p} + bL^{-2} + cL^{-2+y'_p}. \quad (22)$$

The fit yields $y'_p = -0.40$ (3), $R_{e1} = 0.96477$ (3) and $p_{c1} = 0.9996$ (6), consistent with the values found from the fit of the data at $p = 1$, and in good agreement with the expected value $p_{c1} = 1$.

Furthermore, we investigate whether the numerical data for $n = 2$ are consistent with the existence of a marginal fixed point at $p = 1$. Integrating the renormalization flow, Eq. (21), for $n = 2$, and setting the finite size L equal to the rescaling factor e^l ,

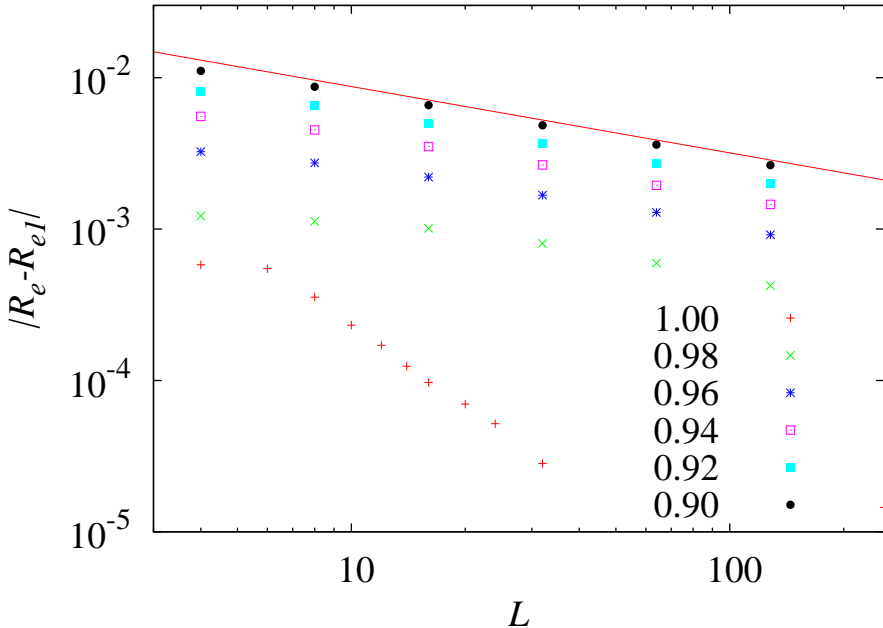


Figure 8. Spanning probability, shown as $|R_e - R_{e1}|$ for $n = 1.5$ vs. system size L , using logarithmic scales, for several values of the bond-occupation probability p . Different symbols correspond with different values of p as listed in the figure. The value $R_{e1} = 0.964780$ was taken from the least-squares fit. For comparison, we show a straight line with a slope $y'_p = -0.4386$, describing the finite-size dependence due to a correction to scaling associated with the irrelevant field along the p direction.

one finds the renormalized value $\Delta p'$ as

$$\Delta p' = \frac{\Delta p}{1 - r_1 \Delta p \ln L} . \quad (23)$$

The corresponding finite-size-scaling equation for the spanning probability is $R_e(\Delta p, L, u) = R_e(\Delta p', 1, L^{y_i} u)$, where u is an irrelevant field and y_i its renormalization exponent. Substitution of $\Delta p'$, and expansion of the scaling function in small arguments, yields

$$R_e(\Delta p, L, u) = R_{ec} + R_1 \Delta p' + R_2(\Delta p')^2 + \dots + b_1 L^{y_i} \quad (24)$$

The numerical data for R_e were fitted by this formula, and several variations of it, concerning the number of irrelevant fields, and the degree in $\Delta p'$. The data for small Δp reveal the existence of only one irrelevant field, with an exponent y_i close to -2 . With this exponent fixed at $y_i = -2$, we obtain fits with satisfactory residuals for the data with $R_e \geq 0.74$. The fits deteriorate for cutoffs at smaller values, apparently because the expansion parameter $\Delta p'$ in Eq. (24) becomes too large. We find that $R_{ec} = R_{e1} = 0.8168$ (5) at the marginal fixed point for $n = 2$, and that it lies at $\Delta p_c \equiv 1 - p_c = -0.001 \pm 0.002$, in agreement with the expected location $p_c = 1$. These data are included in Table 1.

4.4. Numerical representation of the percolation threshold

For a description of the numerical estimates of the percolation thresholds as a function of n , we impose three conditions:

- (1) $\Delta n \propto (\Delta p)^2$ for $\Delta n \rightarrow 0$;
- (2) $\Delta p = 1/\sqrt{3}$ for $\Delta n = 1$;
- (3) $\Delta p = 1 - 2 \sin(\pi/18)$ for $n \rightarrow 0$.

These conditions are based on the exact values given in Sec. 2, which are supported and, for condition (1), supplemented by our numerical evidence. The second condition is a solution of $f_1(\Delta p) \equiv 1 - 2(\Delta p)^2 - 3(\Delta p)^4 = 0$, and the third one of $f_0(\Delta p) \equiv 1 - 3(\Delta p)^2 + (\Delta p)^3 = 0$.

We fitted the $p_c(n)$ data in Table I by the formula

$$\Delta n = \frac{f(\Delta p)}{f_1(\Delta p) + f(\Delta p)}, \quad (25)$$

with $f(\Delta p) \equiv (\Delta p)^2 [2(\Delta p)^3 (4 - \Delta p) + f_0(\Delta p)A(\Delta p)]$, where the amplitude A is a polynomial of Δp —namely, $A(\Delta p) = a_0 + a_1\Delta p + a_2(\Delta p)^2 + \dots$. This equation exactly reproduces $f_1 = 0$ for $\Delta n = 1$ and $f_0 = 0$ for $\Delta n = 2$. From our numerical data $p_c(n)$, we calculated the amplitude $A(\Delta p)$, shown in Fig. 9. The fit for the A data yields $a_0 = 0.488$, $a_1 = 1.493$, and $a_2 = 0.000$. Although a_0 and a_1 lie quite close to the simple fractions $1/2$ and $3/2$, it is very unlikely that they are equal to these values, according to the χ^2 criterion.

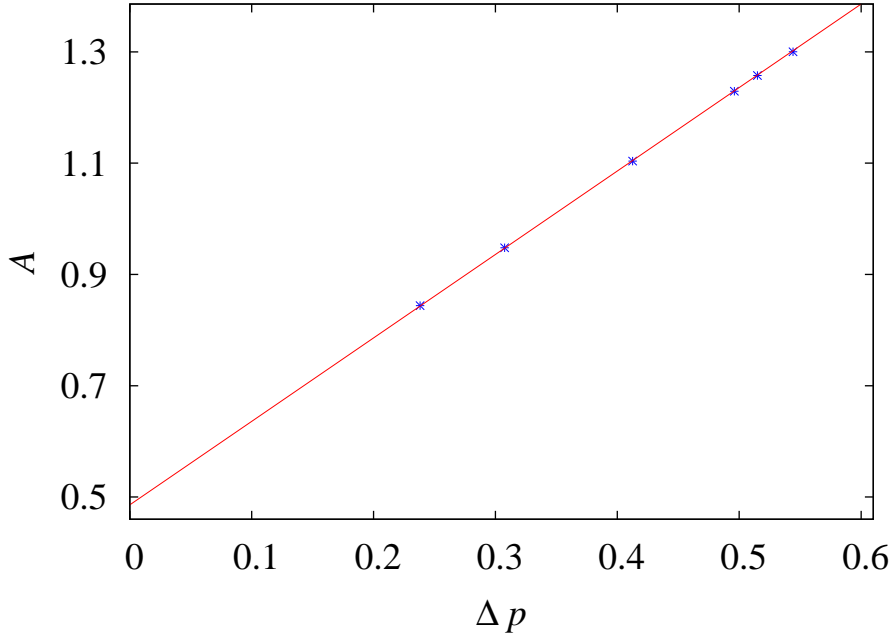


Figure 9. Amplitude A in Eq. (25). The data points are for $n = 1.25$, $\sqrt{2}$, 1.5 , 1.75 , 1.9 , and 1.95 when Δp decreases. The straight line is drawn as $A = a_0 + a_1\Delta p$, with $a_0 = 0.488$ and $a_1 = 1.493$.

We conclude this section with a comment on the condition (1). For $\Delta n > 0$, Eq. (21) yields two fixed points, namely $(\Delta p)_0 = 0$ and $-\sqrt{\Delta n}r_0/r_1$. Expansion

of Eq. (21) near these two fixed points gives the bond-dilution exponents $y'_p = r_0\sqrt{\Delta n}$ near $(\Delta p)_0 = 0$ and $y_p = -r_0\sqrt{\Delta n}$ for $(\Delta p)_0 = -r_0\sqrt{\Delta n}/r_1$. Using the relation between g and n and Taylor-expansion of Eq. (7) near $n = 2$, one obtains $y'_p = -2\sqrt{\Delta n}/\pi$ near $(\Delta p)_0 = 0$ and $y_p = 2\sqrt{\Delta n}/\pi$ near $(\Delta p)_0 = -r_0\sqrt{\Delta n}/r_1$. Therefore, one has $r_0 = -2/\pi$. The amplitudes r_0 and r_1 relate to a_0 in Eq. (25) as $a_0 = (r_1)^2/(r_0)^2$.

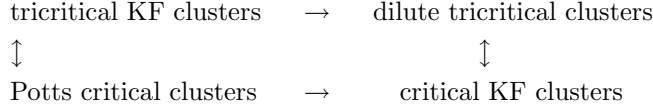
Table 1. Numerical results (N) for the percolation threshold p_c , the bond dilution exponent y_p , and the fractal dimension y_h of the percolation problem on critical $O(n)$ loop configurations. In the absence of intersections as in Fig. 3, the entry for p_c at $n = 2$ was roughly estimated from Fig. 5. Theoretical predictions(T) are included where available.

n		p_c	y_p	R_{ec}	y_h (from P_∞)	y_h (from χ_G)
1.00	N	0.42265 (1)	0.542 (2)	0.5660 (2)	1.8749 (2)	1.8750 (1)
	T	0.422649	0.5416	-	15/8	15/8
1.25	N	0.45587 (2)	0.475 (1)	0.6018 (2)	1.8709 (3)	1.8710 (1)
	T	-	0.4753	-	1.87098	1.87098
$\sqrt{2}$	N	0.48508 (2)	0.425 (1)	0.6275 (2)	1.8687 (3)	1.8687 (1)
	T	-	0.4250	-	1.86875	1.86875
1.50	N	0.50403 (1)	0.395 (2)	0.6420 (2)	1.8678 (2)	1.8678 (1)
	T	-	0.3955	-	1.86775	1.86775
1.75	N	0.58745 (4)	0.290 (3)	0.6932 (2)	1.8658 (3)	1.8660 (1)
	T	-	0.2882	-	1.86603	1.86603
1.90	N	0.6924 (2)	0.186 (5)	0.7402 (3)	1.8668 (4)	1.8670 (1)
	T	-	0.1882	-	1.86700	1.86700
1.95	N	0.7621 (5)	0.13 (1)	0.7650 (5)	1.868 (1)	1.8684 (2)
	T	-	0.1355	-	1.86845	1.86845
2.00	N	1.001 (2)	-0.01 (2)	0.817 (1)	1.8750 (3)	1.87500 (1)
	T	1	0	-	15/8	15/8

5. Conclusion and Discussion

According to the evidence presented in Sec. 2, the dual clusters defined in the critical $O(n)$ loop model should have the universal properties of KF and Potts clusters in the tricritical Potts model, under the condition that the $O(n)$ loop model and the tricritical q -state Potts model have the same conformal anomaly, which implies that $q = n^2$. Thus we also deduced that dilution of the dual clusters in the $O(n)$ loop model by means of a bond-percolation process leads to a percolation transition with the same universal properties as the ‘geometric’ fixed point of diluted KF clusters in the tricritical Potts model [9]. Moreover, these universal properties should also be the same as KF clusters in the critical q -state Potts model, again under the condition that the conformal anomaly is the same. The subsequent numerical verification in Sec. 3 confirms these predictions in satisfactory detail. The diagram below shows the universal relations between the various systems by means of vertical arrows, and the effect of dilution is indicated by horizontal arrows.

$$\begin{array}{ccc}
 \text{O}(n) \text{ dual clusters} & \xrightarrow{\quad} & \text{dilute O}(n) \text{ dual clusters} \\
 \uparrow & & \uparrow
 \end{array}$$



Acknowledgments

We are much indebted to Bernard Nienhuis for valuable discussions. This research is supported by the National Science Foundation of China under Grant #10675021, by the Science Foundation of The Chinese Academy of Sciences, and by the Beijing Normal University through a grant as well as support from its HSCC (High Performance Scientific Computing Center). YD also thanks the support by the Program for New Century Excellent Talents in University (NCET).

- [1] E. Domany, D. Mukamel, B. Nienhuis and A. Schwimmer, Nucl. Phys. B **190**, 279 (1981).
- [2] H. E. Stanley, Phys. Rev. Lett. **20**, 589 (1968).
- [3] B. Nienhuis, Phys. Rev. Lett. **49**, 1062 (1982).
- [4] M. E. Fisher, Physics (N. Y.) **3**, 25 (1967).
- [5] P. W. Kasteleyn and C. M. Fortuin, J. Phys. Soc. Jpn. **46**, (Suppl), 11 (1969).
- [6] C. M. Fortuin and P. W. Kasteleyn, Physica **57**, 536 (1972).
- [7] A. Coniglio and W. Klein, J. Phys. A **13**, 2775 (1980).
- [8] C. Vanderzande, J. Phys. A **25**, L75 (1992).
- [9] Y. Deng, H. W. J. Blöte and B. Nienhuis, Phys. Rev. E **69**, 026123 (2004).
- [10] H. W. J. Blöte, Y. M. M. Knops, and B. Nienhuis, Phys. Rev. Lett. **68**, 3440 (1992).
- [11] B. Nienhuis, A. N. Berker, E. K. Riedel, and M. Schick, Phys. Rev. Lett. **43**, 737 (1979).
- [12] B. Nienhuis, Physica **177**, 109 (1991).
- [13] W. Janke and A. M. Schakel, Nucl. Phys. B **700**, 385 (2004).
- [14] For reviews, see e.g. M. P. Nightingale in *Finite-Size Scaling and Numerical Simulation of Statistical Systems*, ed. V. Privman (World Scientific, Singapore 1990), and M. N. Barber in *Phase Transitions and Critical Phenomena*, eds. C. Domb and J. L. Lebowitz (Academic, New York 1983), Vol. 8.
- [15] Y. Deng, T. M. Garoni, W.-A. Guo, H. W. J. Blöte and A. D. Sokal, Phys. Rev. Lett. **98**, 120601 (2007).
- [16] B. Duplantier, J. Stat. Phys. **49**, 411 (1987).
- [17] H. Saleur and B. Duplantier, Phys. Rev. Lett. **58**, 2325 (1987).
- [18] B. Duplantier and H. Saleur, Phys. Rev. Lett. **63**, 2536 (1989).
- [19] B. Nienhuis, in *Phase Transitions and Critical Phenomena*, edited by C. Domb and J. Lebowitz, (London, Academic 1987) Vol. 11.
- [20] C.-X. Ding, Y. Deng, W.-A. Guo, X.-F. Qian and H. W. J. Blöte, J. Phys. A **40**, 3305 (2007).
- [21] V. S. Dotsenko and V. A. Fateev, Nucl. Phys. B **240**, 312 (1984).
- [22] H. W. J. Blöte, J. L. Cardy and M. P. Nightingale, Phys. Rev. Lett. **56**, 742 (1986).
- [23] B. Nienhuis, J. Phys. A **15**, 199 (1982).
- [24] A. Coniglio, Phys. Rev. Lett. **62**, 3054 (1989).
- [25] R. F. M. Houtappel, Physica **16**, 425 (1950).
- [26] R. H. Swendsen and J. S. Wang, Phys. Rev. Lett. **58**, 86 (1987).
- [27] U. Wolff, Phys. Rev. Lett. **62**, 361 (1989).
- [28] D. Stauffer and A. Aharony, *Introduction to percolation theory* (Taylor and Francis, London, 1991).
- [29] J.-P. Hovi and A. Aharony, Phys. Rev. E **53**, 235 (1996).
- [30] H. T. Pinson, J. Stat. Phys. **75**, 1167 (1994).
- [31] R. M. Ziff, Lorentz, Kleban Physica A **266**, 17 (1999).
- [32] M. F. Sykes and J. W. Essam, J. Math. Phys. **5**, 1117 (1964).
- [33] J. W. Essam in *Phase Transitions and Critical Phenomena*, edited by C. Domb and M. S. Green (Academic Press, London, 1987), Vol. 2, p. 197.
- [34] X.-F. Qian, Y. Deng, and H. W. J. Blöte, Phys. Rev. B **71**, 144303 (2005).